Higher-than-ballistic conduction of viscous electron flows

Haoyu Guo[a], Ekin Ilseven[a], Gregory Falkovich[b,c], and Leonid S. Levitov[a,1]

[a]Department of Physics, Massachusetts Institute of Technology, Cambridge, MA 02139; [b]Department of Physics, Weizmann Institute of Science, Rehovot 76100, Israel; and [c]Institute for Information Transmission Problems, Moscow 127994, Russia

Edited by Allan H. MacDonald, The University of Texas at Austin, Austin, TX, and approved January 24, 2017 (received for review July 25, 2016)

Strongly interacting electrons can move in a neatly coordinated way, reminiscent of the movement of viscous fluids. Here, we show that in viscous flows, interactions facilitate transport, allowing conductance to exceed the fundamental Landauer's ballistic limit G_{ball}. The effect is particularly striking for the flow through a viscous point contact, a constriction exhibiting the quantum mechanical ballistic transport at $T = 0$ but governed by electron hydrodynamics at elevated temperatures. We develop a theory of the ballistic-to-viscous crossover using an approach based on quasi-hydrodynamic variables. Conductance is found to obey an additive relation $G = G_{\text{ball}} + G_{\text{vis}}$, where the viscous contribution G_{vis} dominates over G_{ball} in the hydrodynamic limit. The superballistic, low-dissipation transport is a generic feature of viscous electronics.

electron hydrodynamics | graphene | strongly correlated systems

Free electron flow through constrictions in metals is often regarded as an ultimate high-conduction charge transfer mechanism (1–5). Can conductance ever exceed the ballistic limit value? Here we show that superballistic conduction is possible for strongly interacting systems in which electron movement resembles that of viscous fluids. Electron fluids are predicted to occur in quantum-critical systems and in high-mobility conductors, so long as momentum-conserving electron–electron (ee) scattering dominates over other scattering processes (6–9). Viscous electron flows feature a host of novel transport behaviors (10–22). Signatures of such flows have been observed in ultraclean GaAs, graphene, and ultrapure $PdCoO_2$ (23–26).

We will see that electrons in a viscous flow can achieve through cooperation what they cannot accomplish individually. As a result, resistance and dissipation of a viscous flow can be markedly smaller than that for the free-fermion transport. As a simplest realization, we discuss viscous point contact (VPC), where correlations act as a "lubricant" facilitating the flow. The reduction in resistance arises due to the streaming effect illustrated in Fig. 1, wherein electron currents bundle up to form streams that bypass the boundaries, where momentum loss occurs. This surprising behavior is in a clear departure from the common view that regards electron interactions as an impediment for transport.

A simplest VPC is a 2D constriction pictured in Fig. 1*A*. The interaction effects dominate in constrictions of width w exceeding the carrier collision mean free path l_{ee} (and much greater than the Fermi wavelength λ_F). The VPC conductance, evaluated in the absence of impurity scattering, scales as a square of the width w and inversely with the electron viscosity η,

$$G_{\text{vis}}(w) = \frac{\pi n^2 e^2 w^2}{32\eta}, \quad w \gg l_{\text{ee}}, \qquad [1]$$

where n and e are the carrier density and charge. In the opposite limit, $l_{\text{ee}} \gg w$, the ballistic free-fermion model (1, 5) predicts the conductance $G_{\text{ball}} = 2e^2/h\, N$, where $N \approx 2w/\lambda_F$ is the number of Landauer's open transmission channels. The conductance G_{vis} grows with width faster than G_{ball}. Therefore, for large enough w, viscous transport yields G values above the ballistic bound.

Conveniently, both regimes are accessible in a single constriction, because transport is expected to be viscous at elevated temperatures and ballistic at $T = 0$. The crossover temperature can be estimated in terms of the ee scattering mean free path as

$$l_{\text{ee}}(T)/w = \pi^2/16 \approx 0.62. \qquad [2]$$

This relation is found by setting $R_{\text{vis}} = R_{\text{ball}}$ and expressing viscosity as $\eta = \nu nm = \frac{1}{4} v_F l_{\text{ee}} nm$, where m is the carrier mass and the kinetic viscosity ν is estimated in Eq. S21. The condition Eq. **2** can be readily met in micron-size graphene junctions.

Several effects of electron interactions on transport in constrictions were discussed recently. Refs. 14 and 15 study junctions with spatially varying electron density and, using the time-dependent current density functional theory, predict a suppression of conductance. A hydrodynamic picture of this effect was established in ref. 16. In contrast, here we study junctions in which, in the absence of applied current, the carrier density is approximately position-independent. This situation was analyzed in ref. 27 perturbatively in the ee scattering rate, finding a conductance enhancement that resembles our results.

The relation Eq. **1** points to a simple way to measure viscosity by the conventional transport techniques. Precision measurements of viscosity in fluids date as far back as the 19th century (28). They relied, in particular, on measuring resistance of a viscous fluid discharged through a narrow channel or an orifice, a direct analog of our constriction geometry. Further, viscosity-induced electric conduction has a well-known counterpart in the kinetics of classical gases, where momentum exchange between atoms results in a slower momentum loss and a lower resistance of gas flow. Viscous effects are responsible, in particular, for a dramatic drop in the hydrodynamic resistance upon a transition from Knudsen to Poiseuille regime. For a viscous flow through

Significance

Free electron flows through constrictions in metals are often regarded as an ultimate high-conduction charge transfer. We predict that electron fluids can flow with a resistance that is much smaller than the fundamental quantum mechanical ballistic limit for nanoscale electronics. The "superballistic" low-dissipation transport is particularly striking for the flow through a viscous point contact, a constriction exhibiting the quantum mechanical ballistic transport at zero temperature but governed by viscous electron hydrodynamics at a higher temperature. Unlike other mechanisms of low-dissipation transport, for example, superconductivity, the viscous electron flows can be realized at elevated temperatures, granting a new route for the low-power electronics research.

Author contributions: H.G., G.F., and L.S.L. designed research; H.G., E.I., G.F., and L.S.L. performed research; and H.G., G.F., and L.S.L. wrote the paper.

The authors declare no conflict of interest.

This article is a PNAS Direct Submission.

[1]To whom correspondence should be addressed. Email: levitov@mit.edu.

This article contains supporting information online at www.pnas.org/lookup/suppl/doi:10.1073/pnas.1612181114/-/DCSupplemental.

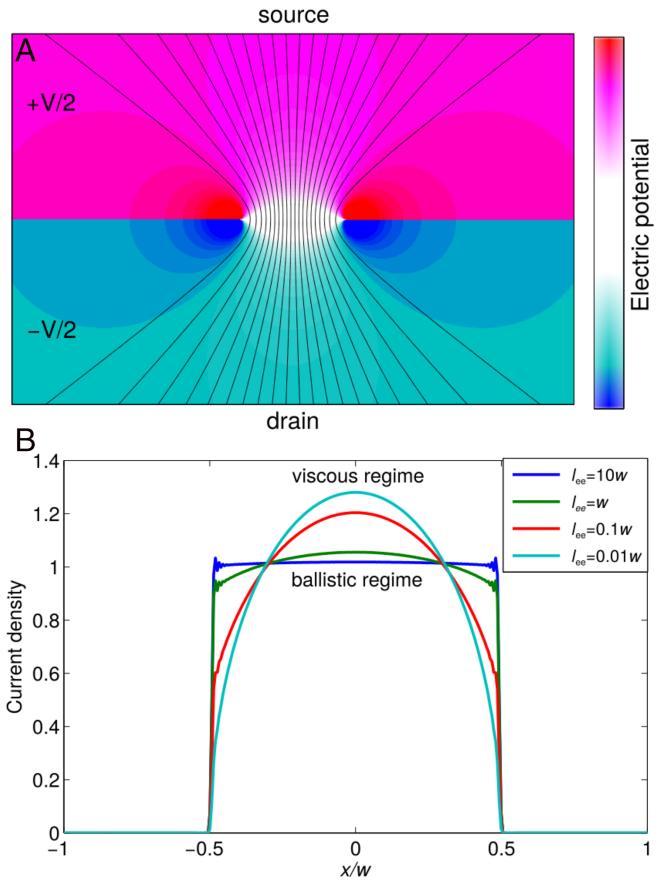

Fig. 1. (*A*) Current streamlines (black) and potential color map for viscous flow through a constriction. Velocity magnitude is proportional to the density of streamlines. Current forms a narrow stream, avoiding the boundaries where dissipation occurs and allowing the resistance, Eq. **1**, to drop below the ballistic limit value. (*B*) Current distribution in the constriction for different carrier collision mean-free-path values. The distribution evolves from a constant in the ballistic regime to a semicircle in the viscous regime, Eq. **10**, illustrating the interaction-induced streaming effect. Parameters used are $L = 3w$ and $b = 10^5 v$. The distributions are normalized to unit total current. A Fourier space filter was used to smooth out the Gibbs phenomenon.

scatterers spaced by a distance L, the typical time of momentum transfer is $\tau \sim L^2/\nu \approx L^2/v_T\ell$, whereas, for an ideal gas, this time is $\tau' = L/v_T$, where v_T is thermal velocity and ℓ is the mean free path. For $\ell \ll L$, the viscous time τ is much longer than the ballistic time τ'.

The peculiar correlations originating from fast particle collisions in proximity to scatterers can be elucidated by a spatial argument: Particle collisions near a scatterer reduce the average velocity component normal to the scatterer surface, $v_\perp$, which slows down the momentum loss rate per particle, $m\mathbf{v}\, v_\perp/L$. Momentum exchange makes particles flow collectively, on average staying away from scatterers and thus lowering the resistance.

The viscosity-induced drop in resistance can be used as a vehicle to overcome the quantum ballistic limit for electron conduction. Indeed, we can compare the values $R_{\rm vis}$ and $R_{\rm ball}$ by putting them in a Drude-like form $R = m/ne^2\tau$, with m as the carrier mass and τ as a suitable momentum relaxation time. Eq. **1** can be modeled in this way using the time of momentum diffusion across the constriction $\tau = w^2/\nu$, whereas $R_{\rm ball}$ can be put in a similar form with $\tau' = w/v_F$ as the flight time across the constriction. Estimating $\nu = \frac{1}{4} v_F l_{\rm ee}$, we see that Eq. **1** predicts resistance below the ballistic limit values so long as $\tau \gtrsim \tau'$, i.e., in the hydrodynamic regime $w \gtrsim l_{\rm ee}$.

Understanding the behavior at the ballistic-to-viscous crossover is a nontrivial task. Here, to tackle the crossover, we use a kinetic equation with a simplified ee collision operator chosen in such a way that the relaxation rates for all nonconserved harmonics of momentum distribution are the same. This model provides a closed-form solution for transport through VPC for any ratio of the length scales w and $l_{\rm ee}$, predicting a simple additive relation

$$G_{\rm VPC} = G_{\rm ball} + G_{\rm vis}. \qquad [3]$$

This dependence, derived from a microscopic model, interpolates between the ballistic and viscous limits, $w \ll l_{\rm ee}$ and $w \gg l_{\rm ee}$, in which the terms $G_{\rm ball}$ and $G_{\rm vis}$, respectively, dominate.

The Hydrodynamic Regime

We start with a simple derivation of the VPC resistance in Eq. **1** using the model of a low-Reynolds electron flow that obeys the Stokes equation (29).

$$(\eta\nabla^2 - (ne)^2\rho)\mathbf{v}(\mathbf{r}) = ne\nabla\phi(\mathbf{r}). \qquad [4]$$

Here $\phi(r)$ is the electric potential, η is the viscosity, and the second term describes ohmic resistivity due to impurity or phonon scattering. Our analysis relies on a symmetry argument and invokes an auxiliary electrostatic problem. We model the constriction in Fig. 1*A* as a slit $-\frac{w}{2} < x < \frac{w}{2}$, $y = 0$. The $y \to -y$ symmetry ensures that the current component j_y is an even function of y whereas both the component j_x and the potential ϕ are odd in y. As a result, the quantities j_x and ϕ vanish within the slit at $y = 0$. This observation allows us to write the potential in the plane as a superposition of contributions due to different current elements in the slit,

$$\phi(x, y) = \int_{-\frac{w}{2}}^{\frac{w}{2}} dx' \mathcal{R}(x - x', y) j(x'), \qquad [5]$$

where the influence function $\mathcal{R}(x, y) = \frac{\beta(y^2 - x^2)}{(x^2+y^2)^2}$ describes potential in a half-plane due to a point-like current source at the edge, obtained from Eq. **4** with no-slip boundary conditions and $\rho = 0$ (30). Here $\beta = \frac{2\eta}{\pi(en)^2}$, and, without loss of generality, we focus on the $y > 0$ half-plane.

Crucially, rather than providing a solution to our problem, the potential-current relation Eq. **5** merely helps to pose it. Indeed, a generic current distribution would yield a potential that is not constant inside the slit. We must therefore determine the functions $j(x)$ and $\phi(x, y)$ self-consistently, in a way that ensures that the resulting $\phi(x, y)$ vanishes on the line $y = 0$ inside the slit. Namely, Eq. **5** must be treated as an integral equation for an unknown function $j(x)$. Denoting potential values at the half-plane $y \geq 0$ edge as $\phi_{+0}(x) = \phi(x, y)_{y=+0}$, we can write the relation Eq. **5** as

$$\phi_{+0}(x) = -\frac{\beta}{2} \int_{-\infty}^{\infty} dx' \left[\frac{j(x')}{(x - x' + i0)^2} + \frac{j(x')}{(x - x' - i0)^2} \right], \qquad [6]$$

where $j(x)$ is the current y component, which is finite inside and zero outside the interval $[-\frac{w}{2}, \frac{w}{2}]$.

A solution of this integral equation such that $\phi_{+0}(x)$ vanishes for all $-\frac{w}{2} < x < \frac{w}{2}$ can be obtained from a 3D electrostatic problem for an ideal-metal strip of width w placed in a uniform external electric field $E_0 = \lambda\hat{\mathbf{x}}$. The strip is taken to be infinite, zero thickness, and positioned in the $Y = 0$ plane such that

$$-\frac{w}{2} < X < \frac{w}{2}, \quad Y = 0, \quad -\infty < Z < \infty \qquad [7]$$

(for clarity, we denote 3D coordinates by capital letters). Potential $\Phi_{3D}(X, Y)$ is a harmonic function, constant on the strip and

behaving asymptotically as $-E_0X$. It is easily checked that the 3D electrostatic problem translates to the 2D viscous problem as

$$\begin{array}{lccc} 3D,\ Y=0: & X & \sigma(X) & E_x(X) \\ & \downarrow & \downarrow & \downarrow \\ 2D,\ y=+0: & x & -\dfrac{\beta}{2}\partial j/\partial x & \phi_{+0}(x) \end{array}. \quad [8]$$

This mapping transforms Coulomb's charge–field relation between the electric field at $Y=0$ and the surface charge density, $E_x(X)=2\int_{-\infty}^{\infty}\frac{\sigma(X')dX'}{X-X'}$, into the 2D viscous relation in Eq. **6**. Potential Φ_{3D}, obtained through a textbook application of conformal mapping, then equals

$$\Phi_{3D}(X,Y)=-\operatorname{Re}\lambda\sqrt{\zeta^2-\frac{w^2}{4}},\quad \zeta=X+iY. \quad [9]$$

Eq. **9** describes the net contribution of the external field E_0 and the charges $\sigma(X)$ induced on the strip. The field component $E_x(X)=-\partial_X\Phi_{3D}$ vanishes on the strip $-\frac{w}{2}<x<\frac{w}{2}$ and equals λ far outside. We can therefore identify λ with $V/2$ in the viscous problem (Fig. 1*A*).

Charge density on the strip, found from **9** with the help of Gauss's law, $\sigma(X)=\frac{\lambda X}{2\pi\sqrt{w^2/4-X^2}}$, under the mapping Eq. **8**, gives a semicircle current distribution,

$$j(|x|<\frac{w}{2})=\frac{\lambda}{\pi\beta}\sqrt{\frac{w^2}{4}-x^2},\quad j\left(|x|>\frac{w}{2}\right)=0. \quad [10]$$

The potential map in Fig. 1*A* is then obtained by plugging this result into Eq. **5**. The flow streamlines are obtained from a similar relation for the stream function (see ref. 30). Evaluating the current $I=\int_{-\frac{w}{2}}^{\frac{w}{2}}j(x)dx=\lambda w^2/8\beta$ and setting $\lambda=V/2$ yields $R=V/I=16\beta/w^2$, which is Eq. **1**. The inverse-square scaling $R\propto w^{-2}$ is distinct from the w^{-1} scaling found in the ballistic free-fermion regime. The scaling, as well as the lower-than-ballistic R values, can serve as a hallmark of a viscous flow.

Potential, inferred from the 2D/3D correspondence, is

$$\phi(x)_{y=\pm 0}=\begin{cases}\dfrac{V|x|}{2\sqrt{x^2-w^2/4}}\operatorname{sgn}y & |x|>\dfrac{w}{2}\\ 0 & |x|<\dfrac{w}{2}\end{cases}, \quad [11]$$

where $\operatorname{sgn}y$ corresponds to the upper and lower sides, $y=\pm 0$. Potential grows toward the slit, diverging at the end points $x=\pm\frac{w}{2}$. This interesting behavior, representing an up-converting DC current transformer, arises due to the electric field pointing against the current near the viscous fluid edge as discussed in ref. 29.

Crossover to the Ballistic Regime

Our next goal is to develop a theory of the ballistic-to-viscous crossover for a constriction. Because we are interested in the linear response, we use the kinetic equation linearized in deviations of particle distribution from the equilibrium Fermi step (assuming $k_BT\ll E_F$),

$$(\partial_t+\mathbf{v}\nabla_{\mathbf{x}})f(\theta,\mathbf{x},t)=I_{\text{ee}}(f)+I_{\text{bd}}(f), \quad [12]$$

where θ is the angle parameterizing particle momentum at the 2D Fermi surface. Here, I_{ee} and I_{bd} describe momentum-conserving carrier collisions and momentum-nonconserving scattering at the boundary, respectively.

In the presence of momentum-conserving collisions, transport is succinctly described by "quasi-hydrodynamic variables" defined as deviations in the average particle density and momentum from local equilibrium (31). These quantities can be expressed as angular harmonics of the distribution $f(\theta,\mathbf{x},t)$,

$$f_0=\langle f(\theta)\rangle_\theta,\quad f_{\pm1}=\left\langle e^{\mp i\theta}f(\theta)\right\rangle_\theta, \quad [13]$$

where we introduced notation $\langle\ldots\rangle_\theta=\oint\ldots\frac{d\theta}{2\pi}$. The quantities f_0 and $f_{\pm1}$, conserved in the ee collisions, represent the zero modes of I_{ee}. For suitably chosen I_{ee}, the task of solving the kinetic equation in a relatively complicated constriction geometry is reduced to analyzing a self-consistency equation for the variables f_0 and $f_{\pm1}$. We will derive a linear integral equation for these quantities and solve it to obtain the current density, potential, and conductance.

To facilitate the analysis, we model I_{ee} by choosing a single relaxation rate for all nonconserved harmonics,

$$I_{\text{ee}}(f)=-\gamma(f-Pf),\quad P=\sum_{m=0,\pm1}|m\rangle\langle m|, \quad [14]$$

where γ represents the ee collision rate, with $l_{\text{ee}}=v/\gamma$, and P is a projector in the space of angular harmonics of $f(\theta)$ that selects the harmonics conserved in ee collisions. Here we introduced Dirac notation for $f(\theta)$ with the inner product $\langle f_1|f_2\rangle=\oint\frac{d\theta}{2\pi}\bar{f}_1(\theta)f_2(\theta)$. Namely,

$$\langle\theta|m\rangle=e^{im\theta},\quad Pf(\theta)=\sum_{m=0,\pm1}\oint\frac{d\theta'}{2\pi}e^{im(\theta-\theta')}f(\theta').$$

As in quantum theory, the Dirac notation proves to be a useful bookkeeping tool to account, on equal footing, for the distribution function position and wavenumber dependence, as well as the angle dependence.

To simplify our analysis, we replace the constriction geometry by that of a full plane, with a part of the line $y=0$ made impenetrable through a suitable choice of $I_{\text{bd}}(f)$. Scattering by disorder at the actual boundary conserves f_0 but not $f_{\pm1}$. We can therefore model momentum loss due to collisions at the boundary using

$$I_{\text{bd}}(f)=-\alpha(x)P'f,\quad \alpha(\mathbf{x})=\begin{cases}0, & |x|<\dfrac{w}{2}\\ b\delta(y), & |x|\geq\dfrac{w}{2}\end{cases}, \quad [15]$$

where P' is a projector defined in a manner similar to P, projecting f on the harmonics $m=\pm1$. The term $\alpha(x)$ describes momentum relaxation on the line $y=0$, equal to zero within the slit and to b outside. The parameter $b>0$ with the dimension of velocity, introduced for mathematical convenience, describes a partially transparent boundary. An impenetrable no-slip boundary, which corresponds to the situation of interest, can be modeled by taking the limit $b\to\infty$.

We will analyze the flow induced by a current applied along the y direction, described by a distribution,

$$f(\theta,\mathbf{x})=f^{(0)}(\theta)+\delta f(\theta,\mathbf{x}),\quad f^{(0)}(\theta)=2j\sin\theta. \quad [16]$$

Here, $f^{(0)}$ and δf, which we will also write as $\left|f^{(0)}\right\rangle$ and $|\delta f\rangle$, represent a uniform current-carrying state and its distortion due to scattering at the $y=0$ boundary. The quantity j is the current density. Once found, the spatial distribution $f(\theta,\mathbf{x})$ will allow us to determine the resulting potential and resistance.
The kinetic equation, Eq. **12**, reads

$$[\partial_t+K+\alpha(\mathbf{x})P']|f\rangle=0,\quad K=\mathbf{v}\nabla+\gamma\hat{1}-\gamma P \quad [17]$$

(from now on, we suppress the coordinate and angle dependence of f and switch to the Dirac notation). Plugging $f=f^{(0)}+\delta f$, we

rewrite Eq. **17** as $(K+\hat{\alpha})\,|\delta f\rangle = -\hat{\alpha}\left|f^{(0)}\right\rangle$, where, for conciseness, we absorbed the projector P' into $\hat{\alpha}$ and set $\partial_t f = 0$ for a steady state. We write a formal operator solution as

$$|\delta f\rangle = -(1+G\hat{\alpha})^{-1} G\hat{\alpha}\left|f^{(0)}\right\rangle, \qquad [18]$$

where $G = K^{-1}$ is the Green's function. Performing analysis in momentum representation, we treat the scattering term in Eq. **15** as an operator,

$$\langle \mathbf{k}|\hat{\alpha}|\mathbf{k}'\rangle = P'\alpha_{k_1-k'_1}, \quad \alpha_k = 2\pi b\delta(k) - bw\,\mathrm{sinc}\,\frac{kw}{2}, \qquad [19]$$

where $\mathrm{sinc}\,x = \frac{\sin x}{x}$. The two terms in α_k describe scattering at the $y=0$ line minus the slit contribution.

Next, we derive a closed-form integral equation for quasi-hydrodynamic variables by projecting the quantities in Eq. **18** on the $m=0,\pm1$ harmonics, Eq. **13**. Acting on Eq. **18** with P gives $|P\delta f\rangle = -(1+\tilde{G}\hat{\alpha})^{-1}\tilde{G}\hat{\alpha}\left|f^{(0)}\right\rangle$, where $\tilde{G} = PGP$ is a 3×3 matrix in the $m=0,\pm1$ space (here we used the identity $\hat{\alpha} = P\hat{\alpha}P$, which follows from $PP' = P'P = P'$). The integral equation is obtained by acting on both sides with the operator $1+\tilde{G}\hat{\alpha}$, giving

$$(1+\tilde{G}\hat{\alpha})\left|\tilde{f}\right\rangle = \left|f^{(0)}\right\rangle. \qquad [20]$$

Here, we defined $\tilde{f} = f^{(0)} + P\delta f$, the full distribution function projected on the $m=0,\pm1$ harmonics.

The quantity $\tilde{f}$ represents an unknown function that can be found, in principle, by inverting the integral operator $1+\tilde{G}\alpha$ in Eq. **20**. However, rather than attempting to invert $1+\tilde{G}\alpha$ directly in 2D, it is more convenient to proceed in two steps: First, analyze Eq. **20** in 1D, on the line $y=0$, and then extend the solution into 2D.

We start with finding $\tilde{G}$. As a first step, we evaluate the 3×3 matrix $S = \gamma P G_0 P$, where $G_0 = 1/(i\mathbf{kv}+\gamma)$. The quantity G_0 is an auxiliary Green's function describing transport in which all harmonics, including $m=0,\pm1$, relax at a rate γ. Direct calculation gives matrix elements (here $m, m' = 0,\pm1$, $\Delta m = m'-m$),

$$S_{mm'} = \left\langle \frac{\gamma e^{i(m'-m)\theta}}{\gamma + i\mathbf{kv}} \right\rangle_\theta = \tanh\beta \frac{e^{i\theta_k \Delta m}}{(ie^{\beta})^{|\Delta m|}}, \qquad [21]$$

where we denote $\sinh\beta = \frac{\gamma}{kv}$ and $\theta_k = \arg(k_1 + ik_2)$.

The matrix $\tilde{G}$ can now be expressed through the matrix S by expanding the actual Green's function as $G = 1/(G_0^{-1} - \gamma P) = G_0 + G_0\gamma P G_0 + ...$, which gives

$$G = G_0 + G_0 T G_0, \quad T = \frac{\gamma P}{1-\gamma P G_0 P}. \qquad [22]$$

Here, we resummed the series, expressing the result in terms of a 3×3 matrix T in a manner analogous to the derivation of the Lippmann–Schwinger T matrix for quantum scattering with a finite number of "active" channels. We note that $\gamma P G_0 P$ is nothing but the matrix S in Eq. **21**. Plugging Eq. **22** into $\tilde{G} = PGP$ and performing a tedious but straightforward matrix inversion, we obtain

$$\tilde{G} = \frac{\gamma^{-1}S}{1-S} = \frac{\sinh\beta}{\gamma}\begin{pmatrix} e^{\beta} & -i\bar{z}_k & -e^{\beta}\bar{z}_k^2 \\ -iz_k & e^{-\beta} & -i\bar{z}_k \\ -e^{\beta}z_k^2 & -iz_k & e^{\beta}\end{pmatrix}, \qquad [23]$$

where $z_k = e^{i\theta_k}$, and the basis vectors are ordered as $|+1\rangle$, $|0\rangle$, and $|-1\rangle$.

In what follows, it will be convenient to transform $|\pm1\rangle$ to the even/odd basis $|c\rangle = \frac{|+1\rangle+|-1\rangle}{\sqrt{2}}$, $|s\rangle = \frac{|+1\rangle-|-1\rangle}{\sqrt{2}i}$. In this basis, $\tilde{G}$ reads

$$\begin{pmatrix} \tilde{G}_{00} & \tilde{G}_{0c} & \tilde{G}_{0s} \\ \tilde{G}_{c0} & \tilde{G}_{cc} & \tilde{G}_{cs} \\ \tilde{G}_{s0} & \tilde{G}_{sc} & \tilde{G}_{ss}\end{pmatrix} = \begin{pmatrix} \frac{R_-}{\gamma\kappa^2} & \frac{-i\sqrt{2}\kappa_1}{\gamma\kappa^2} & \frac{-i\sqrt{2}\kappa_2}{\gamma\kappa^2} \\ \frac{-i\sqrt{2}\kappa_1}{\gamma\kappa^2} & \frac{2\kappa_2^2 R_+}{\gamma\kappa^4} & \frac{-2\kappa_1\kappa_2 R_+}{\gamma\kappa^4} \\ \frac{-i\sqrt{2}\kappa_2}{\gamma\kappa^2} & \frac{-2\kappa_1\kappa_2 R_+}{\gamma\kappa^4} & \frac{2\kappa_1^2 R_+}{\gamma\kappa^4}\end{pmatrix}, \qquad [24]$$

where the basis vectors are ordered as $|0\rangle$, $|c\rangle$, and $|s\rangle$ and we defined $R_\pm(\kappa) = \sqrt{\kappa^2+1}\pm1$ and $\kappa_{1,2} = \frac{v}{\gamma}k_{1,2}$, $\kappa = \sqrt{\kappa_1^2+\kappa_2^2}$. The quantities G and $\tilde{G}$ represent, through their dependence on $\mathbf{k}$, translationally invariant integral operators in position representation and diagonal operators in momentum representation.

Next, we evaluate the matrix that represents the operator $\tilde{G}$ restricted to the line $y=0$,

$$D(k_1) = \int_{-\infty}^{\infty}\frac{dk_2}{2\pi}\tilde{G}(k_1,k_2). \qquad [25]$$

The matrix elements $\tilde{G}_{0c}$ and $\tilde{G}_{0s}$ are odd in k_2 and therefore give zero upon integration in Eq. **25**; as a result we obtain a block diagonal matrix,

$$D(k_1) = \begin{pmatrix} D_{00}(k_1) & D_{0c}(k_1) & 0 \\ D_{c0}(k_1) & D_{cc}(k_1) & 0 \\ 0 & 0 & D_{ss}(k_1)\end{pmatrix}. \qquad [26]$$

The quantity $D_{ss}(k_1)$ will play a central role in our analysis. Indeed, because the flow of interest is symmetric under $y\to-y$ and $x\to-x$, the $\tilde{f}_0$ and $\tilde{f}_c$ components vanish on the $y=0$ line. As a result, the distribution function at $y=0$ is of a pure $|s\rangle$ form, that is, $\tilde{f}(\theta,x) = g(x)\sqrt{2}\sin\theta$.

Evaluating the integral over k_2 in Eq. **25**, we obtain

$$D_{ss}(k) = \frac{\frac{\pi}{2}\,\mathrm{sgn}\,\kappa + \kappa + (\kappa^2+1)\cot^{-1}\kappa}{\pi\kappa v}, \qquad [27]$$

where $\kappa = kv/\gamma$. This expression defines an even function of k with the asymptotics

$$D_{ss}(|k|v \ll \gamma) = \frac{\gamma}{|k|v^2}, \quad D_{ss}(|k|v \gg \gamma) = \frac{2}{\pi v}. \qquad [28]$$

Because the matrix element D_{ss} is an eigenvalue of D for the eigenvector $|s\rangle$, the θ dependence can be factored out of Eq. **20**, giving $(1+D\alpha)\,|g\rangle = \left|g^{(0)}\right\rangle$. Finally, multiplying by D^{-1}, we obtain the "central equation,"

$$D_{ss}^{-1}(k)g_k + \int\frac{dk'}{2\pi}\alpha_{k-k'}g_{k'} = 2\pi\mu\delta(k), \qquad [29]$$

where μ is an unspecified number, akin to a Lagrange multiplier, which fixes the total current value. Here, we wrote the relation $(D^{-1}+\alpha)\,|g\rangle = \mu\,|k=0\rangle$ as an integral equation, replacing k_1 with k for clarity.

The origin of the μ-term in Eq. **29**, and its relation with the properties of the operator D, is simplest to understand using a discretized momentum representation. Letting $k_1 = \frac{2\pi}{L}n$ and replacing

$$\int dk_1 ... \to \frac{2\pi}{L}\sum_n ..., \quad 2\pi\delta(k) \to L\delta_{k,0}, \qquad [30]$$

PHYSICS

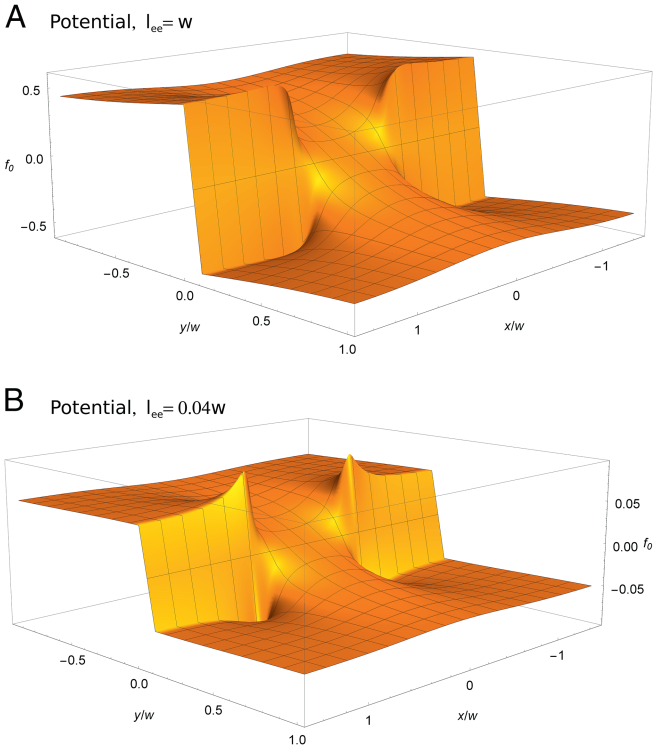

Fig. 2. Potential distribution induced by a unit current through a constriction (*A*) at the crossover, $l_{ee} \approx w$, and (*B*) in the viscous regime, $l_{ee} \gg w$. The spikes at the constriction edges in *B* are a signature of a hydrodynamic behavior (Eq. **11** and accompanying text). Plotted is particle density deviation from equilibrium, $f_0(\mathbf{x})$, which is proportional to potential (see discussion preceding Eq. **33**). Parameters used are (*i*) $\gamma = v/w$ and (*ii*) $\gamma = 15v/w$; other parameter values are the same as in Fig. 1*B*.

that is, putting the problem on a cylinder of circumference L, we see that the values $\tilde{G}_{ss}(k_1, k_2)$ vanish for $k_1 = 0$ and any k_2. This observation implies that the quantity $D_{ss}(k_1)$ also vanishes for $k_1 = 0$, and thus the operator D does not have an inverse. In this case, caution must be exercised when multiplying by D^{-1}. Namely, the quantities $D^{-1}|f\rangle$ are defined modulo a null vector of D, which is the $k_1 = 0$ mode with an unspecified coefficient, represented by the μ-term. We note, parenthetically, that discretization has no impact on the values $D_{ss}(k_1 \neq 0)$ given in Eqs. **27** and **28**.

We obtain current distribution by solving, numerically, Eq. **29**, discretized as in Eq. **30**, and subsequently Fourier-transforming g_k to position space (*Supporting Information*). A large value $b = 10^5 v$ was used to ensure that current vanishes outside the interval $[-\frac{w}{2}, \frac{w}{2}]$. The resulting distribution, shown in Fig. 1*B*, features interesting evolution under varying γ: Flat at small γ, the distribution gradually bulges out as γ increases, peaking at $x = 0$ and dropping to zero near $x = \pm\frac{w}{2}$. In the limit $\gamma \gg v/w$, it evolves into a semicircle coinciding with the hydrodynamic result, Eq. **10**. Current suppression near the constriction edges is in agreement with the streaming picture discussed in the Introduction.

The solution on the line $y = 0$ can now be used to determine the solution in the bulk. For example, to obtain the density $f_0(\mathbf{x})$, we project the relation Eq. **20** on $m = 0$ harmonic, taking into account that both $f^{(0)}$ and $\alpha\tilde{f}$ are of an $|s\rangle$ form. This procedure yields an expression for the 2D density of the form $f_0(\mathbf{x}) = -\int dx' \tilde{G}_{0s}(\mathbf{x}, x')\alpha(x')g(x')$, with $\mathbf{x}$ being a 2D coordinate and $-\infty < x' < \infty$. To avoid handling the $b \to \infty$ limit in α, we write this relation, using Eq. **29**, as

$$f_0(\mathbf{x}) = -\int dx' \tilde{G}_{0s}(\mathbf{x}, x') \left[\mu - \left(D_{ss}^{-1} g\right)(x')\right]. \quad [31]$$

Plugging in $\tilde{G}_{0s}(\mathbf{k}) = \frac{-i\sqrt{2}k_2}{v(k_1^2+k_2^2)}$, Fourier-transforming, and carrying out the k_2 integral by the residue method, $\int dk_2 e^{ik_2 y} \frac{ik_2}{k_1^2+k_2^2} = -\pi e^{-|yk_2|}\text{sgn}\, y$, we obtain

$$f_0(\mathbf{x}) = \frac{\text{sgn}\, y}{\sqrt{2}v} \int \frac{dk_1}{2\pi} e^{ik_1 x - |k_1 y|}[D_{ss}^{-1}(k_1) g_{k_1} - 2\pi\mu\delta(k_1)]. \quad [32]$$

The resulting distributions, shown in Fig. 2, are step-like. At large y, the μ-term dominates, giving $f_0(|\mathbf{x}| \gg w) \approx -\frac{\mu}{\sqrt{2}v}\,\text{sgn}\, y$. Therefore, the step height equals $\frac{\sqrt{2}}{v}\mu$ regardless of the parameter values used.

This relation provides a route to evaluate resistance. Namely, because of charge neutrality, the density f_0 obtained from a noninteracting model translates directly into potential distribution $\phi(\mathbf{x}) = \frac{1}{e\nu_0} f_0(\mathbf{x})$, where ν_0 is the density of states. Dividing the potential difference $V = \frac{\sqrt{2}\mu}{e\nu_0 v}$ by the total current $I = \int dx g(x) \langle ev \sin\theta | s\rangle = \frac{ev}{\sqrt{2}} g_{k_1=0}$ yields a simple expression for resistance,

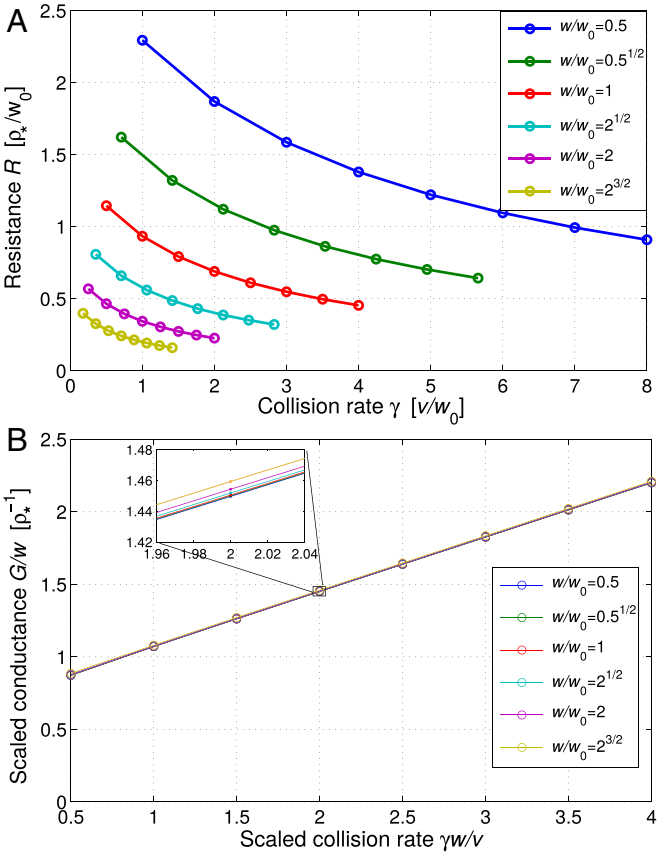

Fig. 3. (*A*) The resistance *R*, Eq. **33**, plotted vs. γ. Upon rescaling $R \to Rw$, $\gamma \to \gamma w$, all of the curves collapse on one curve, confirming that the only relevant parameter is the ratio $w/l_{ee} = w\gamma/v$. (*B*) Scaled conductance $G = 1/(Rw)$ vs. γw. All curves collapse onto a single straight line, which can be fitted with $(0.694 + 0.378\gamma w)\rho_*^{-1}$. This dependence matches Eq. **3** which corresponds to $(2/\pi + \pi/8\gamma w)\rho_*^{-1}$. Parameters used are $b = 10^6 v$, the number of sampling points within the constriction ≈160, and the length unit $w_0 = \frac{1}{30}L$.

$$R = \frac{\mu\rho_*}{v g_{k=0}}, \quad \rho_* = \frac{2}{e^2 v \nu_0}, \qquad [33]$$

where $g_{k=0} = \int g(x)dx$, and ρ_* is a quantity of dimension Ohm · cm. Because $g \propto \mu$, the resulting R values are μ-independent. Fig. 3*A* shows R plotted vs. γ. As expected, R decreases as γ increases, i.e., carrier collisions enhance conduction.

As a quick sanity check on Eq. **33**, we consider the near-collisionless limit $\gamma \ll v/w$. In this case, $D_{ss}(k) \approx 2/\pi v$, and the integral Eq. **29** turns into an algebraic equation, which is solved by a step-like distribution,

$$g(|x| > w/2) = \frac{2\mu}{\pi v + 2b}, \quad g(|x| < w/2) = \frac{2\mu}{\pi v}. \qquad [34]$$

In the limit $b \to \infty$, the total current is $I = \frac{ev}{\sqrt{2}} \frac{2w\mu}{\pi v}$. Taking the 2D density of states $\nu_0 = \frac{Nm}{2\pi\hbar^2}$ (here N is spin–valley degeneracy, e.g., $N = 4$ for graphene), we find

$$R = \frac{V}{I} = \frac{1}{N}\frac{h}{e^2}\frac{\lambda_F}{2w}, \quad \lambda_F = \frac{2\pi}{k_F}. \qquad [35]$$

This result coincides with the collisionless Landauer conductance value. Spatial dependence can be obtained by plugging $g(x)$ into Eq. **32**. Integrating and taking the limit $b \to \infty$ gives

$$f_0(\mathbf{x}) = -\frac{\operatorname{sgn} y}{\sqrt{2}v}\mu\left[1 - \frac{1}{\pi}\theta(\mathbf{x})\right], \qquad [36]$$

where $\theta(\mathbf{x}) = \tan^{-1}\frac{|y|w}{x^2+y^2-\frac{1}{4}w^2}$ is the angle at which the interval $[-\frac{w}{2}, \frac{w}{2}]$ is seen from the point $\mathbf{x} = (x, y)$. This result confirms the value $\frac{\mu}{\sqrt{2}v}$ for the step height.

The dependence R vs. γ shows several interesting features, some expected and some unexpected. First, on general grounds, we expect that the dependence on γ is controlled solely by the ratio w/l_{ee}. Indeed, plotting the rescaled quantity Rw vs. γw, we find a family of curves that all collapse on one curve (this universality only holds at large b, cf. Fig. S1). Second, quite remarkably, inverting this quantity and plotting $1/(Rw)$ vs. γw, we find a nearly perfect straight line with a positive offset at $\gamma = 0$; see Fig. 3*B*. The straight line, which is identical for all w values, is described by $\rho_*/(Rw) = a_1 + a_2\gamma w$. This dependence translates into a simple addition rule for conductance, $G = G_{\text{ball}} + G_{\text{vis}}$. The term G_{ball} describes a γ-independent ballistic contribution that scales linearly with w, whereas G_{vis} describes a viscous contribution proportional to γ that scales as w^2; the two terms yield values $a_1 = 2/\pi$ and $a_2 = \pi/8$, respectively. This finding is in good agreement with the values $a_1 = 0.694$ and $a_2 = 0.378$ obtained from a best fit to the data in Fig. 3*B*.

The additive behavior of conductance at the ballistic-to-viscous crossover comes as a surprise and, to the best of our knowledge, is not anticipated on simple grounds. It is also a stark departure from the Matthiessen's rule that mandates an additive behavior for resistivity in the presence of different scattering mechanisms, as observed in many solids (32). This rule is, of course, not valid if the factors affecting transport depend on each other, because individual scattering probabilities cannot be summed unless they are mutually independent. The independence is certainly out of question for momentum-conserving ee collisions that do not, by themselves, result in momentum loss but can only impact momentum relaxation due to other scattering mechanisms. Furthermore, the addition rule for conductance, Eq. **3**, describes a striking "anti-Matthiessen" behavior: Rather than being suppressed by collisions, conductance exceeds the collisionless value.

ACKNOWLEDGMENTS. We thank M. Reznikov for useful discussions and acknowledge support of the Center for Integrated Quantum Materials (CIQM) under NSF Award 1231319 (to L.S.L.); partial support by the US Army Research Laboratory and the US Army Research Office through the Institute for Soldier Nanotechnologies, under Contract W911NF-13-D-0001 (to L.S.L.); The US-Israel Binational Science Foundation (L.S.L.); MISTI MIT-Israel Seed Fund (L.S.L. and G.F.); the Israeli Science Foundation Grant 882 (to G.F.); and the Russian Science Foundation Project 14-22-00259 (to G.F.).

1. Sharvin YuV (1965) A possible method for studying Fermi surfaces. *Sov Phys JETP* 21:655–656.
2. van Wees BJ, et al. (1988) Quantized conductance of point contacts in a two-dimensional electron gas. *Phys Rev Lett* 60:848–850.
3. Wharam DA, et al. (1988) One-dimensional transport and the quantization of the ballistic resistance. *J Phys C* 21:L209–L214.
4. Maslov DL, Stone M (1995) Landauer conductance of Luttinger liquids with leads. *Phys Rev B* 52:R5539–R5542.
5. van Houten H, Beenakker CWJ (1996) Quantum point contacts. *Phys Today* 49(7): 22–27.
6. Gurzhi RN (1968) [Hydrodynamic effects in solids at low temperature]. *Usp Fiziol Nauk* 94:689–718.
7. Lifshitz EM, Pitaevskii LP (1981) *Physical Kinetics* (Pergamon, New York).
8. Jaggi R (1991) Electron-fluid model for the dc size effect. *J Appl Phys* 69:816–820.
9. Damle K, Sachdev S (1997) Nonzero-temperature transport near quantum critical points. *Phys Rev B* 56:8714–8733.
10. Sheehy DE, Schmalian J (2007) Quantum critical scaling in graphene. *Phys Rev Lett* 99:226803.
11. Fritz L, Schmalian J, Müller M, Sachdev S (2008) Quantum critical transport in clean graphene. *Phys Rev B* 78:085416.
12. Müller M, Schmalian J, Fritz L (2009) Graphene: A nearly perfect fluid *Phys Rev Lett* 103:025301.
13. Mendoza M, Herrmann HJ, Succi S (2011) Preturbulent regimes in graphene flow. *Phys Rev Let* 106:156601.
14. Sai N, Zwolak M, Vignale G, Di Ventra M (2005) Dynamical corrections to the DFT-LDA electron conductance in nanoscale systems. *Phys Rev Lett* 94:186810.
15. Roy D, Vignale G, Di Ventra M (2011) Viscous corrections to the resistance of nano-junctions: A dispersion relation approach. *Phys Rev B* 83:075428.
16. Andreev AV, Kivelson SA, Spivak B (2011) Hydrodynamic description of transport in strongly correlated electron systems. *Phys Rev Lett* 106:256804.
17. Forcella D, Zaanen J, Valentinis D, van der Marel D (2014) Electromagnetic properties of viscous charged fluids. *Phys Rev B* 90:035143.
18. Tomadin A, Vignale G, Polini M (2014) Corbino disk viscometer for 2D quantum electron liquids. *Phys Rev Lett* 113:235901.
19. Narozhny BN, Gornyi IV, Titov M, Schütt M, Mirlin AD (2015) Hydrodynamics in graphene: Linear-response transport. *Phys Rev B* 91:035414.
20. Principi A, Vignale G, Carrega M, Polini M (2016) Bulk and shear viscosities of the 2D electron liquid in a doped graphene sheet. *Phys Rev B* 93:125410.
21. Cortijo A, Ferreirós Y, Landsteiner K, Vozmediano MAH (2015) Hall viscosity from elastic gauge fields in Dirac crystals. *Phys Rev Lett* 115:177202.
22. Lucas A, Crossno J, Fong KC, Kim P, Sachdev S (2016) Transport in inhomogeneous quantum critical fluids and in the Dirac fluid in graphene. *Phys Rev B* 93(7):075426.
23. de Jong MJM, Molenkamp LW (1985) Hydrodynamic electron flow in high-mobility wires. *Phys Rev B* 51:13389–13402.
24. Bandurin DA, et al. (2016) Negative local resistance caused by viscous electron backflow in graphene. *Science* 351:1055–1058.
25. Crossno J, et al. (2016) Observation of the Dirac fluid and the breakdown of the Wiedemann-Franz law in graphene. *Science* 351(6277):1058–1061.
26. Moll PJW, Kushwaha P, Nandi N, Schmidt B, Mackenzie AP (2016) Evidence for hydrodynamic electron flow in $PdCoO_2$. *Science* 351(6277):1061–1064.
27. Nagaev KE, Ayvazyan OS (2008) Effects of electron-electron scattering in wide ballistic microcontacts. *Phys Rev Lett* 101:216807.
28. Marvin RS (1971) The accuracy of measurements of viscosity of liquids. *J Res Natl Bur Stand Sect A* 75A(6):535–540.
29. Levitov L, Falkovich G (2016) Electron viscosity, current vortices and negative nonlocal resistance in graphene. *Nat Phys* 12:672–676.
30. Falkovich G, Levitov L (2016) Linking spatial distributions of potential and current in viscous electronics. arXiv:1607.00986.
31. Levinson IB (1977) Boundary conditions in phonon hydrodynamics. *JETP* 46:165–172.
32. Blatt FJ (2014) *Matthiessen's Rule* (McGraw-Hill, New York).